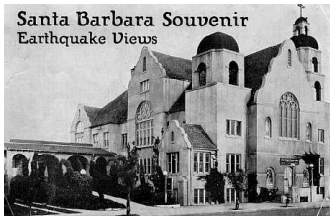

4th IASPEI / IAEE International Symposium:

Effects of Surface Geology on Seismic Motion

August 23–26, 2011 · University of California Santa Barbara

PROBABILISTIC SEISMIC HAZARD MAPS FOR SEATTLE: 3D SEDIMENTARY BASIN EFFECTS, NONLINEAR SITE RESPONSE, AND UNCERTAINTIES FROM RANDOM VELOCITY VARIATIONS

Arthur Frankel

U.S. Geological Survey
University of Washington
Box 351310
Seattle WA 98195
USA

William Stephenson, David Carver, Jack Odum, Robert Williams, and Susan Rhea
U.S. Geological Survey
Box 25046
Denver, CO 80225
USA

ABSTRACT

We have produced probabilistic seismic hazard maps of Seattle for 1 Hz spectral acceleration using 541 finite-difference simulations with a 3D velocity model. Simulations with the 3D model reproduced the observed amplification for sites in the Seattle basin caused by basin surface waves and by focusing of S-waves at the southern edge of the basin. The seismic hazard calculation used the earthquake recurrence parameters in the U.S. national seismic hazard maps. Finite-fault simulations were conducted for earthquakes on the Seattle and Southern Whidbey Island faults. Simulations for point sources on the Cascadia subduction zone were used to quantify the amplification expected for great subduction zone earthquakes. We used empirical factors based on Vs30 to account for the nonlinear amplification of soft-soil sites on artificial fill and Holocene alluvium. We evaluated the effects of 3D random spatial variations in shear-wave velocity added to the 3D model on simulations of M6.7 earthquakes on the Seattle fault at the southern edge of the Seattle basin. We considered random models with a von Karman correlation function and a 10% standard deviation of seismic velocity in the top 1.3 km and 5% standard deviation from 1.3-10.8 km depth. These models can produce variations of over a factor of 2 in peak ground velocity and spectral acceleration, over distances of only a few km. The random variations tend to reduce the peak ground motions of basin surface waves in areas with the highest amount of forward rupture directivity and increase the amplitude in other directions.

INTRODUCTION

In order to improve the accuracy and utility of probabilistic seismic hazard assessment (PSHA) it is important to include nonlinear site response, 3D sedimentary basin effects, and earthquake rupture directivity. In 2007, we released probabilistic urban seismic hazard maps for Seattle that incorporated these phenomena through the use of hundreds of 3D ground-motions simulations (Frankel et al. 2007). The first part of this paper summarizes the procedure used to construct these maps and describes the maps. A key aspect of PSHA is the incorporation of uncertainties from randomness (aleatory) and lack of knowledge (epistemic). The second portion of this paper describes our recent work quantifying the effects of the uncertainty in the 3D velocity model arising from small-scale 3D random variations in seismic velocities.

We have documented the importance of basin surface waves and basin-edge focusing on seismograms recorded in the Seattle basin from the 2001 M6.8 Nisqually earthquake and other earthquakes (Frankel et al., 2002a and 2009; Stephenson et al., 2006). Figure 1 is a map of the Puget Sound region highlighting the area of the Seattle hazard maps, the locations of the Seattle basin and Seattle fault zone, and the epicenters of earthquakes used to validate the 3D model. Figure 2 contains maps showing the amplification at 1 Hz for various sites, relative to a rock site outside of the basin, from an inversion of the Fourier spectra of 19 earthquakes and from spectra of the Nisqually earthquake. The results are similar between the two datasets. The highest amplification (factor of 3-7) is observed for sites on soft soil (fill and alluvium). Significant amplification of about a factor of two is observed on stiff soil sites (Pleistocene age glacial deposits) within the Seattle basin, even though the Vs30 at these sites is similar to those for rock sites outside the basin. This

amplification is largely caused by the presence of basin surface waves and is observed to vary with the azimuth of the incoming waves (Frankel et al. 2009). Figure 3 depicts the observed velocity seismograms filtered around 1 Hz from the Nisqually earthquake, documenting the large basin surface waves that are generated from conversion of incident S-waves at the southern edge of the Seattle basin. These basin surface waves are the largest arrivals for the 1 Hz velocity waveforms recorded at these Seattle basin sites (about 60 km epicentral distance), despite the large depth of the Nisqually earthquake (52 km). These surface waves were also documented and modeled at longer periods by Pitarka et al. (2004).

Stephenson (2007) constructed a 3D velocity model of the region, including the Seattle basin, using results from seismic tomography, seismic refraction and reflection studies, gravity surveys, and boreholes. Frankel et al. (2009) validated the 3D model by successfully modeling the observed 1 Hz amplification, amplitudes, and longer period waveforms from several earthquakes using the 3D finite difference simulations. The 3D model does not include the relatively thin layers of soft soils. We consider the amplification from these soils in a separate set of calculations.

SEISMIC HAZARD MAPS

The procedure used to make the Seattle hazard maps is shown in Figure 4. 541 3D finite difference simulations were used to make the maps, which depict 1 sec pseudo spectral acceleration (S.A.) with 5% critical damping. Hazard curves were calculated for 7236 sites with 280m spacing. Approximately 7.8 million synthetic seismograms were analyzed to make the maps. We considered earthquake sources on the Seattle fault, Southern Whidbey Island fault (SWIF), and Cascadia subduction zone (CSZ), as well as background shallow and deep earthquakes. See Frankel et al. (2007) for more details. For each 3D simulation, we constructed maps of amplification of 1 Hz spectral acceleration, relative to rock sites outside the basin. These maps contain the 3D basin effects, as well as the effects of rupture directivity for the Seattle fault and the SWIF. These amplification maps were then used to amplify the ground-motion values predicted at each site from ground-motion prediction equations (GMPE's) for a firm-rock site condition. The Seattle maps used the same set of GMPE's applied in the 2002 U.S. National Seismic Hazard Maps (NSHM; Frankel et al., 2002b), before applying basin and directivity effects. The maps apply the fault-recurrence and seismicity parameters from the 2002 NSHM's to get the earthquake rates in the PSHA calculation.

The annual frequency $\lambda(u \geq u_0)$ of exceeding ground motion u_0 at site i from multiple faults or source locations was determined by summing over source location and magnitude:

.

$$\lambda(u \geq u_0) = \sum_{M} \sum_{\text{source}_j} \text{rate}(M, \text{source}_j) P(u \geq u_0 | \text{site}_i, \text{source}_j, M)$$

Here $P(u \geq u_0 \mid site_i, source_j, M)$ is the probability of having ground motions u greater or equal to u_0 at site i, if an earthquake occurs at source location j with magnitude M. Here u is the 1 sec S.A.. To calculate u we start with the ground motion $u_{rock}(M,D)$ derived from generic rock-site GMPE (e.g., Abrahamson and Silva, 1997). Then we calculate the site- and source-specific amplification using the 3D simulations, so that

$$u = u_{rock}(M,D) A_{3D}(\text{site}_i, \text{source}_j) .$$

Here $A_{3D}(site_i, source_j)$ is the amplification of the 1 sec S.A. for each site and source, derived from each 3D simulation by taking the geometrical average of the 1 sec S.A. from the two horizontal synthetic seismograms at each site and dividing them by the 1 sec S.A. averaged at three reference rock sites outside the Seattle basin. These amplification terms include basin-edge focusing and basin-edge generated surface waves. Note that this "amplification" term also contains rupture directivity effects for the Seattle fault and SWIF simulations.

For soft-soil sites we also apply nonlinear amplification factors, since the relatively thin layer of soft soils is not contained in the 3D velocity model. Now the 1 sec S.A. u is determined from

$$u = u_{rock}(M,D) A_{3D}(\text{site}_i, \text{source}_j) A_{soft}(\text{site}_i, PGA_{rock}) \quad ,$$

where $A_{soft}(site_i, PGA_{rock})$ is the nonlinear amplification of the soft-soil site, with respect to the spectral accelerations determined for

the top of the 3D velocity model. The nonlinear amplification depends on the PGA at that site for a rock site condition. We first developed a map of the thickness of fill and/or alluvium based on a compilation of borehole data (K. Troost, written comm.. 2006). Based on a generic shear-wave velocity profile for these sites (Williams et al., 1999) and the thickness of soft-soil deposits, we constructed a map of estimated Vs30. Then we applied the nonlinear empirical amplification factors of Choi and Stewart (2005) to determine $A_{soft}(site_i, PGA_{rock})$. In the future, 3D nonlinear calculations should be performed for a 3D model that includes the soft soils.

Note that the calculation of $P(u \geq u_0 \mid site_i, source_j, M)$ requires the aleatory uncertainty in the ground motions at a particular site from a specific source. We used the aleatory uncertainty of the GMPE's applied for the rock-site ground-motion calculations. By considering the ground motions from various sources we are essentially adding the randomness from azimuthally-variable basin effects and rupture directivity effects that are not well-represented in the GMPE's. Another approach would be to conduct a much more extensive set of simulations that varied hundreds of parameters to directly estimate the aleatory uncertainty (e.g., Graves et al., 2010).

The 3D simulation code was written by Pengcheng Liu and is a 4th order finite-difference code that utilizes a finer grid spacing in the shallow portion of the grid (Liu and Archuleta, 2002). We use a grid spacing of 70m in the top 1.4 km of the grid and 210m below that, although a coarser vertical spacing is applied at deeper depths. The minimum shear-wave velocity of the 3D model is 600 m/s, similar to the measured Vs30 for the glacially-overridden soils that dominate much of the Seattle area.

Approximately 460 simulations were done for earthquakes between M6.6 and 7.1 on the Seattle fault, which is a major contributor of hazard for Seattle. Figure 5 shows results from two of the simulations with different random distributions for slip on the fault surface. We used slip distributions where the spectral amplitude is proportional to k^{-2}, where k is wave number. The maps in Figure 5 document the basin edge focusing at the southern edge of the Seattle basin, the higher amplitudes caused by basin surface waves, and the forward rupture directivity. The simulations included rupture zones that were distributed along the length of the Seattle fault and along the three traces for the fault zone identified by Blakely et al. (2002). Three different hypocenters and slip distributions were considered for each rupture scenario. Each hypocenter and slip distribution combination is considered as a scenario in the PSHA, and additional aleatory variability is applied to the ground motions from each scenario. The Seattle fault dips to the south and the hypocenters (rupture initiation points) are located at the base of the fault, so that rupture proceeds up dip, generally to the north. The mean rupture velocity is independent of depth, with a random component added.

The expected basin amplification for great earthquakes on the CSZ was estimated using 3D simulations for point sources on various locations of the CSZ. These amplification patterns vary with the location of rupture zones along the CSZ. We also consider a set of finite fault simulations for earthquakes on the SWIF. Point-source simulations for earthquakes at various azimuths and depth ranges were conducted to quantify the hazard from background earthquakes (Frankel et al. 2007).

Figure 6 shows a set of hazard maps for 1 Hz S.A. with a 2% probability of exceedance in 50 years. The map on the left is from the NSHM's and assumes a firm-rock site condition. The middle map is based on the 3D simulations and highlights the increased hazard for sites in the Seattle basin. This map shows amplification factors of about a factor of two for these sites, compared to the rock-site map on the left, consistent with the observations depicted in Figure 2. This amplification is caused by the basin amplification and the forward rupture directivity for Seattle fault earthquakes.

For the map on the right (Figure 6) we apply empirical amplification factors to account for the nonlinear amplification at soft soil sites, as described above. The highest hazard sites are soft soil sites within the Seattle basin. Next highest hazard levels are at stiff soil sites within the basin and soft-soil sites outside the basin. The lowest hazard sites at this frequency are locations outside the basin where the bedrock is at shallow depths.

EFFECTS OF 3D RANDOM VELOCITY VARIATIONS

Even with the complexity of the 3D velocity model, it does not contain the small-scale random variations of seismic velocity present in the actual crust. These small-scale spatial fluctuations will scatter, focus, and defocus seismic waves and produce waveform and amplitude variations. Since these small-scale velocity variations are very difficult to map deterministically, they constitute an epistemic uncertainty to the ground-motion calculations. They may also cause systematic changes in the median amplitudes relative to

the velocity model without these realistic variations.

We used 3D velocity variations that follow a von Karman correlation function, such that the power spectrum of the variations is proportional to $(1 + (ka)^2)^{-3/2}$, where a is the correlation distance and k is the radial wave number. This medium has a Hurst exponent of zero. For high wave numbers greater than 1/a (or wavelengths much shorter than a), this type of medium will have a standard deviation of velocity independent of wave number, when it is bandpass filtered over equal logarithmic intervals of wave number (Frankel and Clayton, 1986; Frankel, 1990). Thus, this type of medium will have equal fluctuations of velocity over a wide range of length scales. Frankel and Clayton (1986) found that this type of medium produced realistic fluctuations in amplitude and travel times across seismic arrays and generated realistic levels of seismic coda from scattering. Figure 7 shows slices through a 3D medium with these random fluctuations. The randomized media developed here have a Gaussian probability distribution. Hartzell et al. (2010) studied how 3D random variations affected peak ground motions in 3D simulations for strike-slip earthquakes in the San Francisco Bay area.

The random variations are superimposed on the 3D velocity model for the Puget Sound region. In the simulations we have done so far, we applied the same random seed for the P and S-wave velocities and the densities, so their variations are correlated. We found that adding the random component only to the S-wave velocity and not to the P-wave velocity and density produced very similar results. We constructed a model where the random variations had a standard deviation of velocity of 10% in the top 1.3 km. This encompasses the maximum thickness of the Quaternary sediments in the Seattle basin. This standard deviation in shear-wave velocity is roughly consistent with velocity variations in the Los Angeles basin found by Thelan et al. (2006) using surface methods and the borehole database of Wills and Silva (1998) and Gibbs et al. (2000). For depths between 1.3 and 10.8 km we used a standard deviation of velocity of 5%. We chose a value of a of 5 km to ensure a wide range of wavelengths for the variations; larger correlation distances would produce similar results for this type of random medium. Figure 8 depicts shear wave velocity at a depth of 1.4 km in the original model and the model with the random fluctuations.

We did several 3D simulations for M6.7 earthquakes on the Seattle fault. We considered various random number seeds for the random portion of the model and different random number seeds for the slip distribution on the fault. This thrust fault in the model dips at 45 degrees to the south and generally strikes east-west. The top of rupture is at 3 km depth. For most runs the rupture was initiated at the bottom of the rupture zone midway along its length. Rupture propagates outward and upward from this point. There is a north-south jog in the rupture surface about halfway along its length, which is based on the geometry of the fault inferred from reflection profiles and magnetic anomalies (Blakely et al., 2002).

We find that these random fluctuations produce substantial variations in the peak ground velocities (PGV) and S.A.'s at 1.0 and 3.0 sec, when compared to those for the original model without the fluctuations. Here we determined the PGV's and S.A.'s from the geometrical mean of the PGV's and S.A.'s on the two horizontal components. Figure 9 shows maps of the PGV's from the original and randomized models, using the same rupture history in the two simulations. In the original model there are areas of high PGV for S-waves near the fault plane caused by directivity and patches of high slip on the fault. There are also broad areas of high PGV in parts of the basin that are caused by focusing or constructive interference of basin surface waves generated along the southern edge of the basin by conversion of incident S-waves. Some of these high areas are up dip of patches of high slip on the fault.

The random velocity variations produce PGV and S.A. variations of over a factor of 2 in many cases, relative to the original model. Figure 10 exhibits the ratios of PGV's between the randomized and original models. The ratio map on the right is from the two PGV maps in Figure 9; the map to the left shows the ratios using a different random seed. PGV variations of over a factor of two can occur over distances as small as about 2 kilometers. The randomness in the seismic velocities tends to break down areas of focusing in the original model, especially for surface waves within the Seattle basin. However, scattering by the random velocity variations produces localized areas of high amplitudes that were not present in the synthetics from the original model.

Figure 11 shows examples of velocity synthetics for sites in the basin where the peak velocities differ substantially between the original and randomized models. We found that the basin surface waves are much more affected by the randomness than the S-waves. These surface waves have a longer travel time in the basin sediments than the direct S-wave and, thus, are more affected by the velocity fluctuations within the basin. In some cases the randomized medium focuses the basin surface wave, producing higher peak velocities in localized areas and in other cases it reduces areas of focusing of the surface waves (Figure 11).

Figure 12 contains ratios for 1.0 sec and 3.0 sec S.A. between synthetics from the randomized and original models. Again, there are variations of over a factor of two between the S.A.'s from the randomized model and the original. While the high and low areas are grossly similar between the 1.0 sec and 3.0 sec S.A. ratio maps, the wavelength of the variations is longer for the 3.0 sec S.A. map compared to the 1.0 sec map.

Histograms of the ratios of the 1.0 sec and 3.0 sec S.A.'s between the randomized and original models roughly follow a log normal distribution (Figure 13). The average standard deviation of the natural logarithm of the 1.0 sec S.A. variations is approximately 0.34, based on simulations with various random number seeds. This corresponds to a standard deviation of a factor of 1.4 and is similar to results found for randomized models by Hartzell et al. (2010). Note that there are more sites with low ratios than predicted from a log normal distribution (Figure 13 left). This is caused by the low ratios preferentially observed in the up dip direction. The ratios for 3.0 sec S.A. are fit with a log normal distribution with a standard deviation of about 0.27 (ln units). These standard deviations are a significant fraction of that determined from the misfit of observations with ground-motion prediction equations. For example, the standard deviations of this misfit determined by Campbell and Bozorgnia (2008; their Table 3) for stiff-soil sites are 0.62 and 0.65 (ln units) for 1.0 sec and 3.0 sec S.A., respectively. Thus a significant portion of the so-called aleatory uncertainty in empirically-derived GMPE's may, in some cases, be caused by epistemic uncertainty from the small-scale random variations in the upper crust.

Another key observation from the simulations is that the amplitude tends to be reduced in areas of largest amount of forward rupture directivity. Energy is preferentially scattered out of these areas into areas where the directivity is less. The rectangles in Figure 10 highlight the areas in the forward rupture direction where the randomized medium has reduced amplitude (in blue) compared to the original model. These occur north of the western and eastern portions of the rupture zone. Interestingly, the area between the rectangles shows an average increase of amplitude. The effects of forward directivity for this area would be less than for sites on either side, since the distance along the rupture surface is less for this direction. This area also lies up dip of an inferred north-south jog in the fault trace (Blakely et al., 2002; Johnson et al., 1999) and rupture surface, which may also affect the amplitudes. This pattern is even more apparent in the ratios made for 1.0 and 3.0 sec S.A. (Figure 12).

To better understand the effects of the randomized model on directivity we also did simulations for a fault rupture consisting of only the eastern segment of the previous model. Figure 14 documents how the area of reduced amplitude shifts to the west when the hypocenter is moved from the lower southwest corner of the rupture zone to the midway point at the bottom of the rupture (see rectangles in Figure 14). This confirms that the biggest decreases of amplitude are for directions with the largest expected forward directivity.

Figure 15 shows the PGV's for sites along two east-west lines, for the randomized and original models, based on the simulations for the full fault trace. Note that there are large spatial variations of PGV even in the original model for the line across the Seattle basin (at north-south position of 40 km), due to focusing of basin surface waves and patches of high slip on the fault surface. The randomized model produces variations with smaller length scales of about 2 km and less that are not present in the synthetics from the original model. These types of variations over distances of 2 km or less are often observed in recordings from closely-spaced stations and may also explain localized differences in damage sometimes observed for similar types of buildings. Figure 15 also shows the decrease in amplitude up dip of the eastern edge of the rupture for the randomized model, indicating the loss of energy in areas that have the greatest forward directivity.

CONCLUSIONS

The Seattle urban seismic hazard maps represent a major improvement over maps that apply amplification factors based solely on Vs30. They incorporate the basin amplification that is observed in recordings for the Seattle basin, as well as the directivity of ruptures on the Seattle fault. It is important for future building codes to include the amplification from deep sedimentary basins.

It is also important to characterize the heterogeneity of the seismic velocities in sedimentary basins. This will provide key information on the expected variations of ground motions over short distances and the uncertainties in the median values. This variability of earthquake ground motions should be considered when assessing the response of buildings. It is also important to include realistic random variations in 3D simulations, since they may change the median ground-motion values in some areas from those found in simulations for models without these variations.

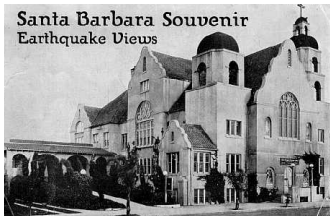

ACKNOWLEDGMENTS

We thank Stephen Hartzell and Robert Graves for their helpful reviews.

REFERENCES

Abrahamson, N.A., and W.J. Silva [1997], Empirical response spectral attenuation relations for shallow crustal earthquakes, Seism. Res. Letts., vol. 68 (1), pp. 94-127.

Blakely, R.J., R.E. Wells, C.S. Weaver, and S.Y. Johnson [2002], Location, structure, and seismicity of the Seattle fault zone, Washington: evidence from aeromagnetic anomalies, geologic mapping, and seismic-reflection data, GSA Bulletin, vol. 114, pp. 169-177.

Campbell, K.W., and Y. Bozorgnia [2008], NGA ground motion model for the geometrical mean horizontal component of PGA, PGV, PGD, and 5% damped PSA at spectral periods between 0.01 s and 10.0 s (2008). Earthquake Spectra, vol. 24, pp. 139-172.

Choi, Y., and Stewart, J.P. [2005], Nonlinear site amplification as function of 30m shear wave velocity, Earthquake Spectra, vol. 21, pp. 1-30.

Frankel, A., and R.W. Clayton [1986], Finite difference simulations of seismic scattering: implications for the propagation of short-period waves in the crust and models of crustal heterogeneity, J. Geophys. Res., vol. 91, pp. 6465-6489.

Frankel, A. [1991], High-frequency spectral falloff of earthquakes, fractal dimension of complex rupture, b value, and the scaling of strength on faults, J. Geophys. Res., vol. 96, pp. 6291-6302.

Frankel, A., D.L. Carver, and R.A. Williams [2002a], Nonlinear and linear site response and basin effects in Seattle from the M 6.8 Nisqually, Washington, earthquake, Bull. Seism. Soc. Am., vol. 92, pp. 2090-2109.

Frankel, A., M. Petersen, C. Mueller, K. Haller, R. Wheeler, E. Leyendecker, R. Wesson, S. Harmsen, C. Cramer, D. Perkins, and K. Rukstales [2002b], Documentation for the 2002 update of the national seismic hazard maps, *U.S. Geol. Surv. Open-File Rept. 02-420*, 39 pages, *http://eqhazmaps.usgs.gov*.

Frankel, A.D., W.J. Stephenson, D.L. Carver, R.A.Williams, J.K. Odum, and S. Rhea [2007], Seismic hazard maps for Seattle incorporating 3D sedimentary basin effects, nonlinear site response, and rupture directivity, *U.S. Geol. Surv. Open-File Rept. 07-1175*, 70 pp.

Frankel, A., W. Stephenson, and D. Carver [2009]. Sedimentary basin effects in Seattle, Washington: ground-motion observations and 3D simulations (2009). Bull. Seism. Soc. Am., vol. 99, pp. 1579-1611.

Gibbs, J. F., J. C. Tinsley, D. M. Boore, and W. B. Joyner [2000]. Borehole velocity measurements and geological conditions at thirteen sites in the Los Angeles, California region, *U.S. Geol. Surv. Open-File Rept. OF 00-470*, 118 pp.

Graves, R., S. Callaghan, E. Deelman, E. Field, T. H. Jordan, G. Juve, C. Kesselman, P. Maechling, G. Mehta, K. Milner, D. Okaya, P. Small, and K. Vahi [2010], CyberShake: Full Waveform Physics-Based Probabilistic Seismic Hazard Calculations for Southern California, PAGEOPH, DOI 10.1007/s00024-010-0161-6.

Hartzell, S., S. Harmsen, and A. Frankel [2010], Effects of 3D random correlated velocity perturbations on predicted ground motions, Bull. Seism. Soc. Am., vol. 100, pp. 1415-1426.

Johnson, S.Y., S. Dadisman, J.R. Childs, J.R., and W.D. Stanley [1999], Active tectonics of the Seattle fault and central Puget Sound, Washington—Implications for earthquake hazards, Geol. Soc. Am. Bull., vol. 111, pp.1042-1053.

Liu, P-C, and R.J. Archuleta [2002], The effect of a low-velocity surface layer on simulated ground motion, Seism. Res. Letts., vol. 73, p. 267.

Pitarka, A., R. Graves, and P. Somerville [2004],Validation of 3D model of Puget Sound region based on modeling ground motion from the 28 February 2001 Nisqually earthquake, Bull. Seism. Soc. Am., vol. 94, pp. 1670-1689.

Stephenson, W. J. [2007], Velocity and density models incorporating the Cascadia Subduction Zone for 3D earthquake ground motion simulation, *U.S. Geol. Surv. Open-File Rept. OF 2007-1348*, 24 pp.

Stephenson, W.J., A.D. Frankel, J.K. Odum, R.A.Williams, and T.L. Pratt [2006], Towards resolving an earthquake ground motion mystery in west Seattle, Washington state: shallow seismic focusing may cause anomalous chimney damage, Geophys. Res. Letts., DOI 10.1029/2005GL025037.

Thelen, W.A., M. Clark, C. T. Lopez, C. Loughner, H. Park, J. B. Scott, S. B. Smith, B. Greschke, and J. N. Louie [2006], A transect of 200 shallow shear-velocity profiles across the Los Angeles basin, Bull. Seism. Soc. Am., vol. 96, pp. 1055-1067.

Waldron, H.H., B.A. Liesch, D.R. Mullineaux, and D.R. Crandell [1962], Preliminary geologic map of Seattle and vicinity, *U.S. Geol. Surv.* Map I-354.

Williams, R.A., W.J. Stephenson, A.D. Frankel, and J.K. Odum, [1999], Surface seismic measurements of near-surface P- and S-wave seismic velocities at earthquake recording stations, Seattle, Washington, Earthquake Spectra, vol. 15, pp. 565-584.

Wills, C. J., and W. Silva [1998], Shear wave velocity characteristics of geologic units in California, Earthquake Spectra, vol. 14**,** pp. 533–556.

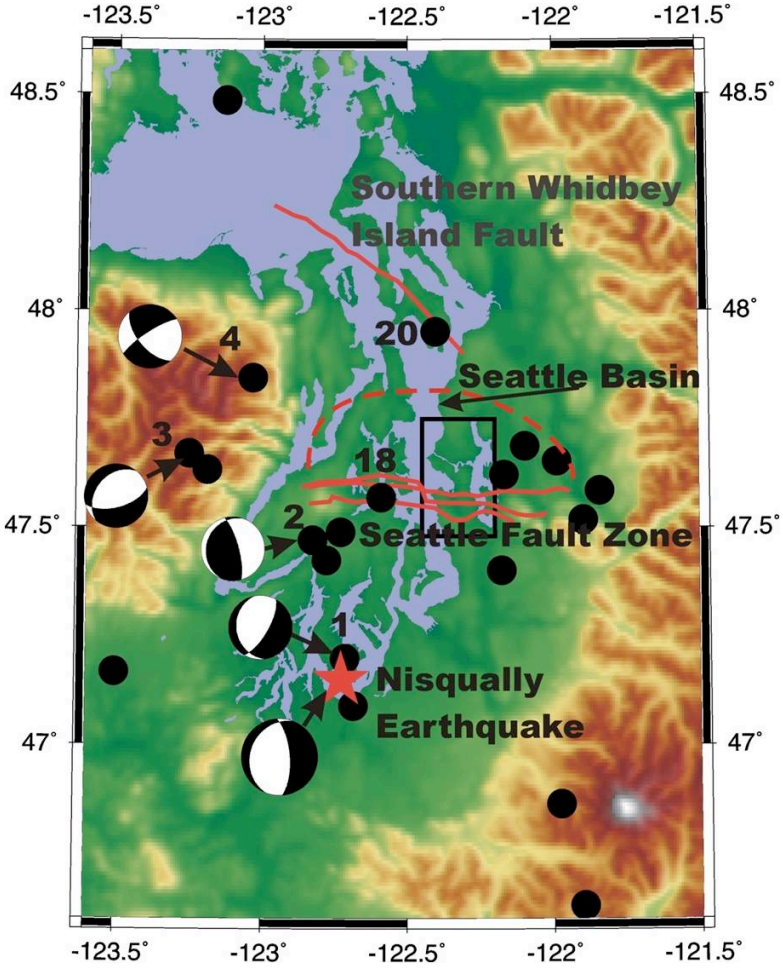

Figure 1. Map of Puget Sound, Washington region from Frankel et al. (2009). Box denotes area of Seattle hazard maps. Dots are epicenters of earthquakes used in inversion for site amplification shown in Figure 2. Focal mechanisms are for events studied to validate the 3D velocity model. Star is the epicenter of the 2001 M6.8 Nisqually earthquake (depth= 52 km). Seattle fault zone forms the southern edge of the Seattle basin.

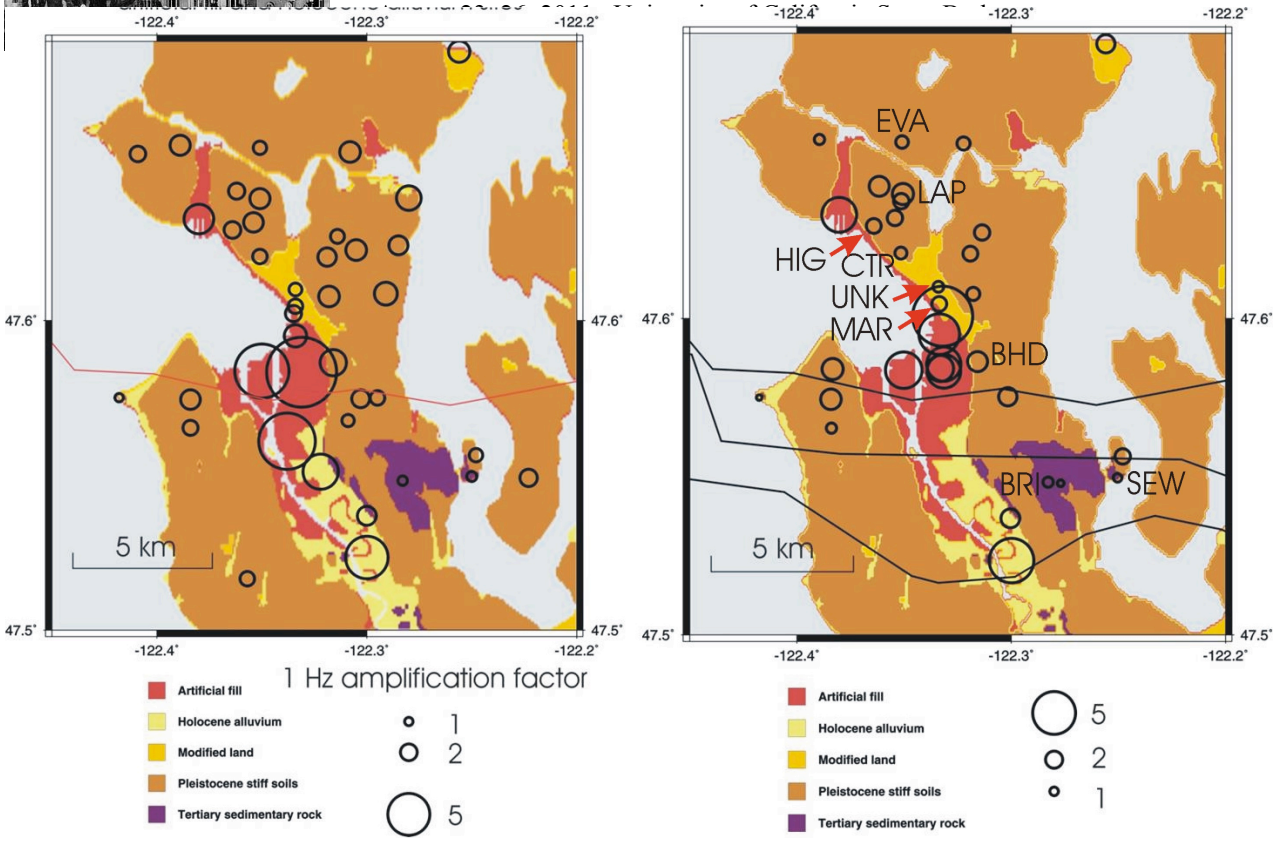

Figure 2. (left) Amplifications at 1 Hz, relative to rock site outside of the basin, derived from an inversion of 19 earthquakes M2.5-4.8. Circles are located at station locations and diameter is proportional to amplification. (right) 1 Hz amplification determined from recordings of the M6.8 Nisqually earthquake. Surficial geology from Waldron (1962). Roughly east-west striking lines signify location of Seattle fault zone (Blakely et al., 2002). Areas of soft soil are in red and yellow.

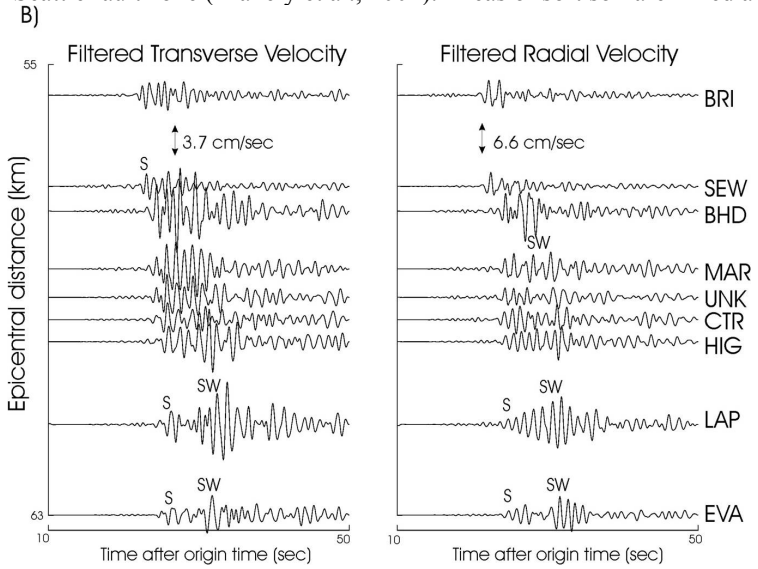

Figure 3. Velocity waveforms of the Nisqually earthquake filtered from 0.67-1.3 Hz for stations along a south to north line (from Frankel et al., 2002a). Station locations shown in Figure 2. Stations BRI and SEW are to the south outside the basin. Note the large basin surface wave (SW) that is generated between SEW and BHD at the southern edge of the Seattle basin.

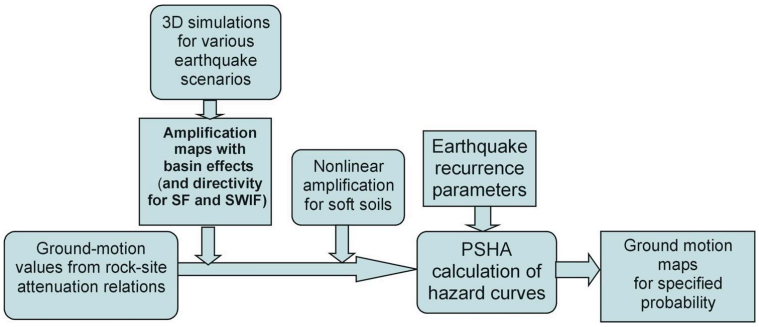

Figure 4. Flowchart of the procedure applied to construct the Seattle urban seismic hazard maps (from Frankel et al., 2007).

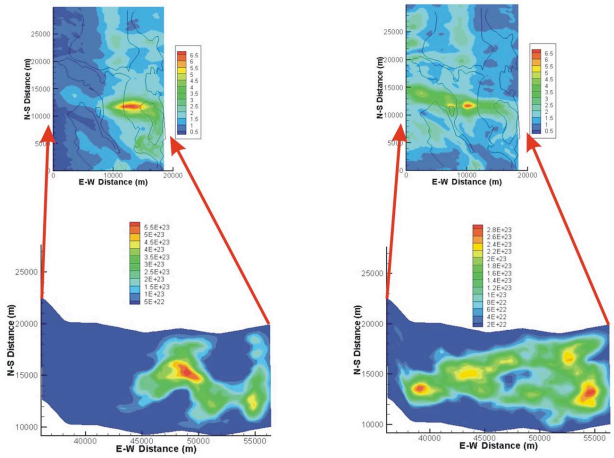

Figure 5. (bottom) Moment release (or slip) along surface of Seattle fault for two different slip realizations for M6.8 earthquakes (from Frankel et al., 2007). Fault surface dips to the south at 45 degrees and rupture initiates at bottom of fault midway along strike. Arrows indicate location of corners of fault surface on maps. (top) Maps of 1 Hz amplification from each 3D simulation, relative to three sites south of the basin. Outline of coast is shown in each map. Note high amplification at southern edge of Seattle basin and high amplitudes up dip of high slip areas on the fault.

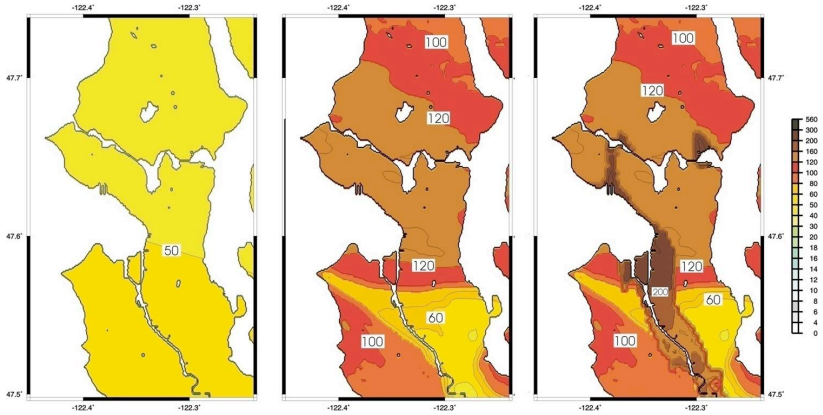

Figure 6. Seismic hazard maps for 1.0 sec spectral acceleration (%g) for 2% probability of exceedance in 50 years (from Frankel et al. (2007). (left) Map for firm-rock site condition from the 2002 National Seismic Hazard Maps. (middle) Map derived from 541 3D simulations, showing the amplification in the Seattle basin. (right) Same as middle map from 3D simulations, but also considering nonlinear amplification for soft-soil sites of fill and alluvium (see surficial geology map in Figure 2).

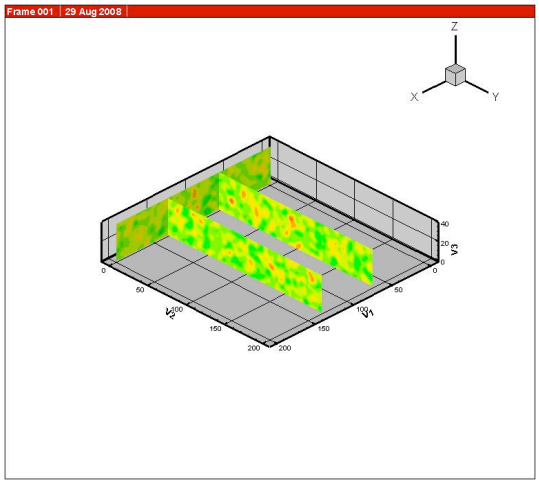

Figure 7. Vertical slices through a 3D random medium with random variations of seismic velocity (colors) that follow a von Karman correlation function.

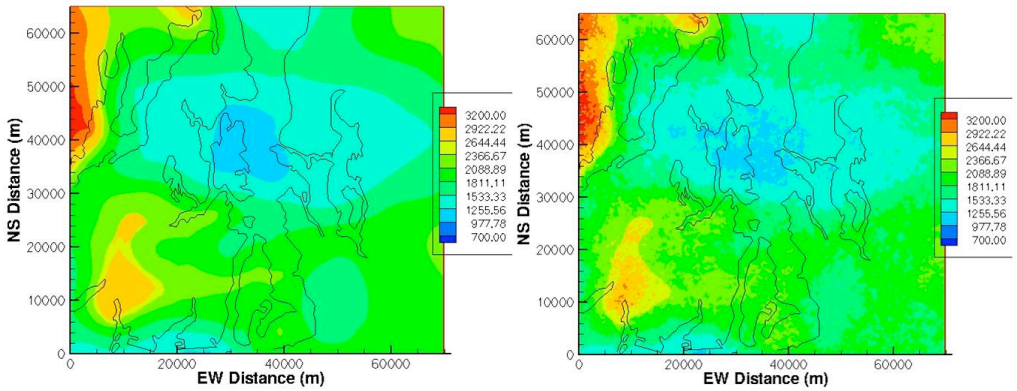

Figure 8. Shear wave velocity (m/s) at 1.4 km depth for (left) the original 3D model and (right) the randomized model.

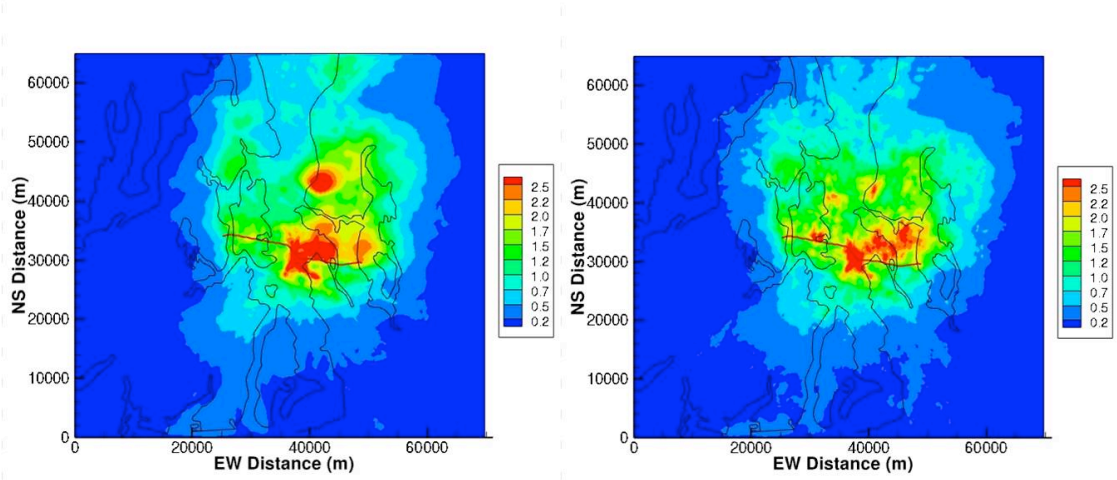

Figure 9. Peak ground velocities (m/s) for simulations for a M6.8 earthquake on the Seattle fault. Roughly east-west line with jog is the fault trace. Coastline is shown in black. (left) PGV for original model and (right) PGV for randomized model. Both simulations have the same slip history on the fault.

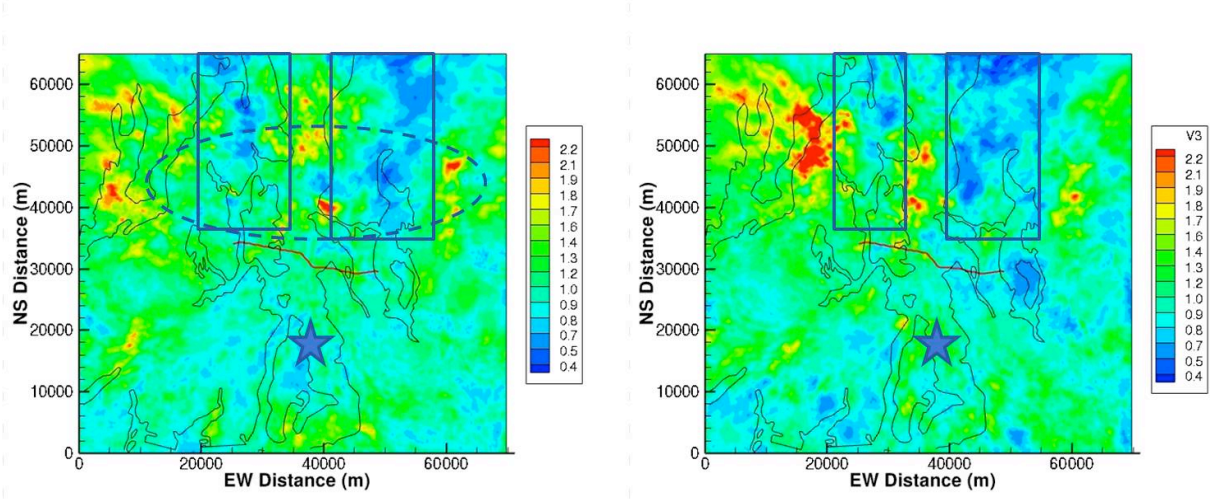

Figure 10. Ratios of PGV's between the randomized model and the original model. Green and red areas are amplified by the randomized model; blue areas are deamplified. Roughly east-west line with jog is the fault trace. Star denotes epicenter of rupture initiation. Dashed ellipse is approximate outline of the Seattle basin. (right) Ratios from two PGV maps shown in Figure 9. (left) Ratios of PGV for a randomized medium with a different random seed. Rectangles denote areas in the forward rupture direction that are deamplified by the randomized medium. There are amplified areas between the rectangles and to the sides.

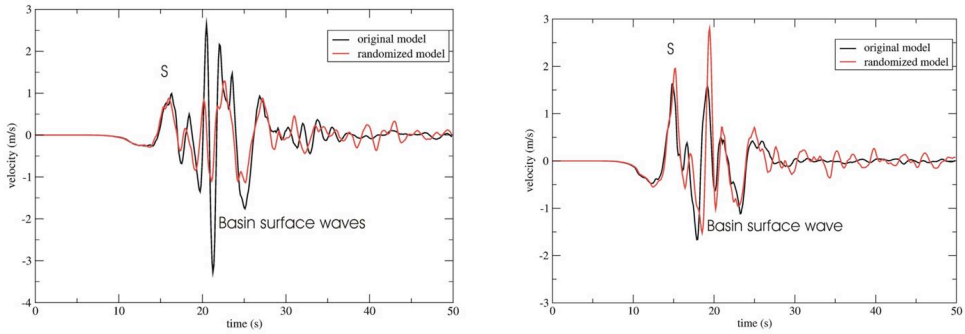

Figure 11. North-south synthetic velocity waveforms at two sites in the Seattle basin showing the difference between the original model (black) and the randomized model (red). (left) Site where the randomized model deamplifies the basin surface wave. (right) Site where the randomized model increases the amplitude of the basin surface wave.

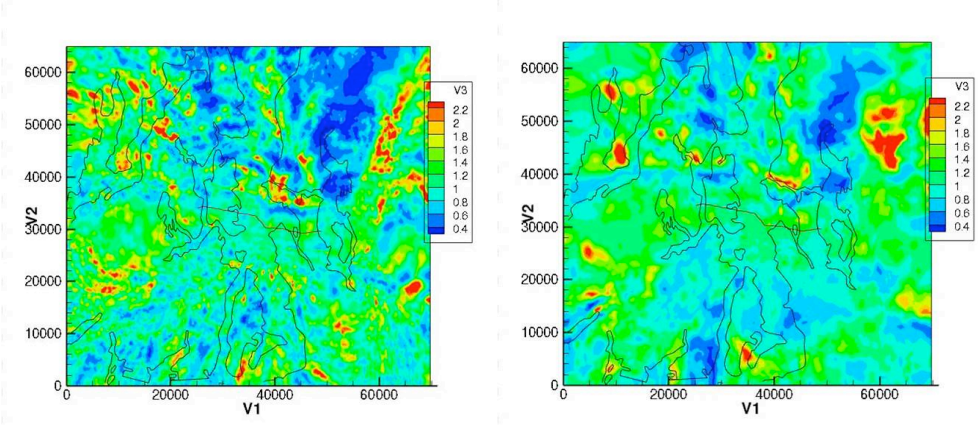

Figure 12. (left) Ratio of 1.0 sec S.A. between randomized and original models. (right) Ratio of 3.0 sec S.A. between randomized and original model. Randomized model is the same for both periods.

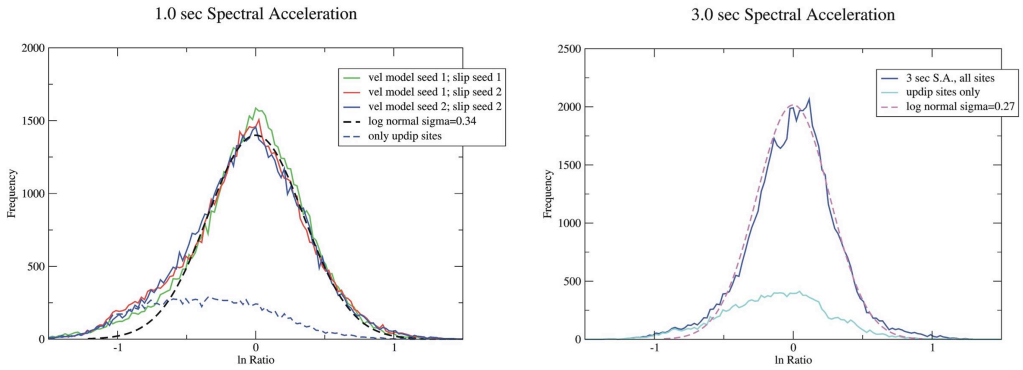

Figure 13. (left) Histograms of 1.0 sec S.A. ratios between randomized and original models. Dashed line is fit for a log normal distribution. Dashed blue line is for sites up dip of rupture. (right) Histogram of ratios 3.0 sec S.A. ratios between randomized and original models and fit to log normal distribution.

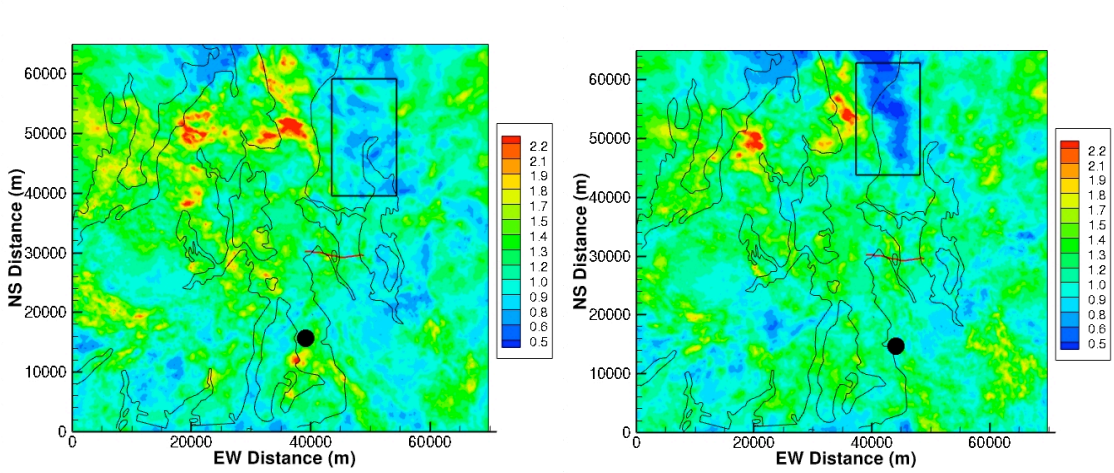

Figure 14. Ratios of PGV's between randomized and original models for simulations for rupture on the eastern portion of the fault segment (east-west line). Dots are epicenters of the rupture initiation. Rectangles denote areas of deamplification. Note how this deamplification area shifts to the west as the epicenter is shifted to the east, following the area of highest forward rupture directivity.

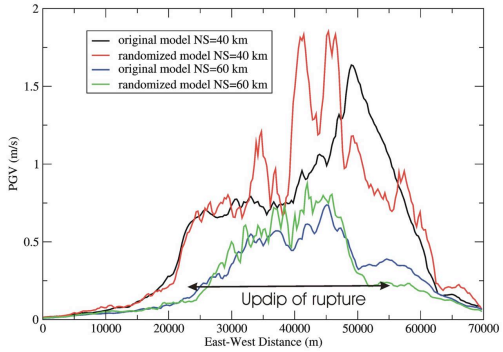

Figure 15. PGV's for two east-west lines of sites, for the simulation shown in left side of Figure 10. Red and black lines are for a line 40 km from the southern edge of the model (see coordinates in Figure 10). Blue and green lines show PGV's for a line 60 km from the southern edge of the model. Note the large variations in PGV over short distances for the randomized model (red line), compared to that from the original model (black). A rougher variation of PGV is also observed for the line at 60 km distance (green) compared to the original model (blue).